A Global Topographic Map of Titan

Ralph D. Lorenz[1], Bryan W. Stiles[2], Oded Aharonson[3], Antoine Lucas[4], Alexander G. Hayes[5], Randolph L. Kirk[6], Howard A. Zebker[7], Elizabeth P. Turtle[1], Catherine D. Neish[8], Ellen R. Stofan[9], Jason W. Barnes[10] and the Cassini RADAR Team

1 Space Department, Johns Hopkins University Applied Physics Laboratory, 11100 Johns Hopkins Road, Laurel, MD 20723, USA

2 Jet Propulsion Laboratory, California Institute of Technology, Pasadena, CA 91109

3 Helen Kimmel Center for Planetary Science, Weizmann Institute of Science, Rehovot, Israel 76100

4 Laboratoire AIM, Université Paris 7/CNRS/CEA, 91191 Gif sur Yvette Cedex, France

5 Cornell University, Ithaca, NY

6 U.S. Geological Survey, Flagstaff, AZ

7 Department of Electrical Engineering, Stanford University, Stanford, CA

18 8 Goddard Space Flight Center, Greenbelt, MD

19 9 Proxemy Research, Rectortown, VA

20 10 University of Idaho, Moscow, ID

21

22 Submitted to Icarus, 29th January 2013

23 Revised version 27th March 2013

24 Accepted 3rd April 2013

Abstract

Cassini RADAR SARtopo and altimetry data are used to construct a global gridded 1x1 degree elevation map, for use in Global Circulation Models, hydrological models and correlative studies. The data are sparse, and so most of the map domain (~90%) is populated with interpolated values using a spline algorithm. The highest (~+520m) gridded point observed is at 48^{o} S, 12^{o} W. The lowest point observed (~1700m below a 2575km sphere) is at 59^{o} S, 317 ^{o}W : this may be a basin where liquids presently in the north could have resided in the past. If the deepest point were once a sea with the areal extent of present-day Ligeia Mare, it would be ~1000m deep. We find four prominent topographic rises, each ~200km wide, radar-bright and heavily dissected, distributed over a ~3000km arc in the southeastern quadrant of Titan (~40-60^{o} S, 15-150^{o} W).

Keywords : Titan, Geological Processes

1. Introduction

Many geological, hydrological and meteorological processes are profoundly affected by topography. To fully understand these processes it is desirable to have a global topographic dataset of high and uniform horizontal and vertical resolution : Mars science was revolutionized by the generation of such data by the laser altimeter instrument MOLA, and lunar science is currently benefiting from the data being generated by the Lunar Orbiter Laser Altimeter (LOLA).

Titan displays a range of fascinating and dramatic meteorological and other processes that are evidently affected by topography on various scales. For example, Lorenz et al. (2008) observed that even an early (and highly incomplete) sampling of Titan's river channels suggested a generally poleward trend in flow direction, which is consistent with initial topography data that showed that the poles are topographically lower than the equator (Zebker et al., 2009a). Lorenz and Radebaugh (2009) showed that the equatorial linear dunes are diverted by topographic highs of 100-300m with slopes of the order of 1/200, but blocked by slopes of 1/50 or more. It is therefore a pity that our knowledge of Titan's topography is and will remain very poor compared with Earth, Mars, Venus and the Moon, where global maps exist. For Titan, such a global dataset must await a future Titan orbiter mission, and radar altimeters have been suggested as priority instruments for such a mission.

While far from global in extent, nor uniform in quality, Cassini radar topography data are now sufficient to assemble a useful topography map at fairly high resolution. Using a smaller subset of these data, Zebker et al. (2009a) determined the low-order shape of Titan's surface with a spherical harmonic analysis, and Lorenz et al. (2011) evaluated Titan's hypsogram. The utility of maps developed from sparse data at Mars was demonstrated pre-MOLA by Smith and Zuber (1996) who studied Mars' shape

using a limited number of Viking orbiter radio occultation heights and groundbased radar tracks and determined the character of the north-south dichotomy.

Recent applications of topography data (which have used the Zebker et al. (2009a) spherical harmonic solutions) include the effects on winds in a Global Circulation Model (GCM) by, Tokano (2010) and the examination of the spatial extent of liquids on Titan as a function of ocean volume (Larsson and McKay, in press 2013). Efforts such as these can benefit from a higher-resolution topography product. Thus. we offer here a documented topographic map product in a convenient form. The product is definitive in that it captures the data available at present and only a few tracks per year will be added subsequently: it may be that no significant update is worthwhile until the completion of the Cassini Solstice Mission in 2017. The map product is available for download in digital form as Supplemental information and at http://www.lpl.arizona.edu/~rlorenz/topomap.html and may additionally be archived in future at the NASA Planetary Data System (PDS).

We offer in this paper only some brief interpretations and observations about the topographic map. Correlative studies with broader datasets and geophysical analyses of topography are left for future work in the interests of making the present data available promptly.

2. Titan Topographic Data

Available topographic data on Titan is discussed at some length in Lorenz et al. (2011). The principal data source here is the synthetic aperture radar (SAR) imaging, which covers approximately 35% of Titan's surface with narrow swaths a couple of hundred km wide. An along-track topographic estimate

profile, named SARtopo, can be generated by exploiting the overlap in the beam footprints used to generate the swath to estimate the terrain height in several bands along the length of the swath (Stiles et al., 2009). Note that high-altitude single-beam SAR imaging has been used to extend the imaging coverage of Titan, but since it has no overlapping beams, provides no direct topography. The dataset presented here is rather more extensive than that used in the construction of Titan's hypsogram in Lorenz et al. (2011) in so far as that study used only the SARtopo dataset for flybys TA-T61. The present dataset through T65 comprises 132 SARTopo tracks (for each SAR imaging flyby, there are typically 3 different topography swaths between the different beam pairs.) Although the posting of individual heights is made quite closely, such that the dataset comprises about 1.3 million datapoints, there is partial overlap between the ~20km wide correlation regions used and so the profiles are oversampled.

Additionally, radar altimetry along 20 short tracks (~300-700km long, Zebker et al., 2009b) has been obtained, plus three long ones : T30, 3600km from high northern latitudes down to the equator near the prime meridian, T49 across Ontario Lacus (e.g. Wye et al., 2009), and T77 along the equator at the Shangri-La/Xanadu boundary. An additional long altimetry swath was acquired by the spacecraft on T60 in August 2009 but was lost due to a Deep Space Network antenna outage. The 23 altimetry tracks through T77 are used, which introduce another ~12,000 datapoints. These data are available via the NASA Planetary Data system as 'Altimeter Summary Files', e.g. 'T77_ABDR_SUMMARY_04_D229_V02.CSV' . The SARtopo data is presently being validated for general use (and indeed during the preparation of this paper, we identified some spurious points in preliminary SARtopo files). Note that we use the 'Corrected First Moment' (or corrected centroid) height estimate, as this is most consistent with the SARtopo heights – see Zebker et al., 2009b for further discussion. Also note that these data include a few points with unphysical surface heights that were acquired when

the spacecraft attitude deviated from nadir during flyby T41 – these points can be excluded by requiring the incidence angle for valid data to be less than 0.7 degrees.

The geographical distributions of the two datasets are presented in figure 1. By design, there are no major unobserved regions on a hemispheric scale, although some gaps ~60^{o} (~2000km) across are unavoidably present due to the distribution of Cassini orbits. When the data are binned in 1x1^{o} latitude-longitude space, the SARtopo data fill 6696 of the 64800 bins (compared with 5400 in Lorenz et al., 2011) and the altimetry adds an additional 770 bins. By this metric, topography data, corresponding to of order 100,000km of tracks, covers about 11% of Titan's surface.

< Figure 1 here >

The binned data are plotted in figure 2 against latitude. The depression of Titan's poles (e.g. Zebker et al., 2009) is clearly seen in both datasets. It is not surprising that the two datasets are generally consistent with each other in that the SARtopo data have been controlled to available altimeter points.

It is of interest to note the extreme values in these data. The highest bin in the altimeter data is at 216^{o}W, 39^{o}N, at 352m, while in the SARtopo it is found at 12^{o}W 48^{o}S, at 520m (note that there is no overlapping altimetry data here for comparison). The minimum elevations found are at 258^{o}W, 61^{o}S (-1049m, altimetry) and 316^{o}W, 59^{o}S (-1712m, SARtopo). Since the SARtopo data are more extensive, it is not surprising that the most extreme values are found in those data. It is noteworthy that the lowest point measured is deep in the southern hemisphere . Note that these are not the extreme values in the original datasets, but are the extreme values of the 1x1^{o} averages, so isolated and small higher and lower points may exist even in the observed areas.

3. Interpolation Scheme

In order to fully populate a map grid, we must interpolate those values where measurements are not present. This is a well-known problem in geophysics, geology and other fields. For the present application, following other geological gridding analyses, we employ the spline technique with tension, which minimizes curvature while maintaining continuous second derivatives (Smith and Wessel, 1990). This approach also avoids the issue that spherical harmonic approaches can insert features where there are no data (e.g. antipodal to large features that are observed). The splining (with tension=0.5) is performed twice, once with conventional cylindrical coordinates, and once with coordinates rotated 90 degrees, such that interpolations across the poles are well-behaved and the two grids blended accordingly. The resulting field (figure 3) is seen to have smooth behavior where there is no data and joins points reasonably.

We confirmed that this approach was robust by comparing with a somewhat heuristic approach of averaging across all azimuths from a point. For the point to be estimated, the data grid is searched in each of 32 equispaced directions until height data is found (or a distance of 60^{o} is exceeded). From this set of up to 32 points, the height estimate is computed by weighting each point by its distance raised to an exponent -2. This conceptually simple approach yields a broadly similar result, confirming the robustness of the major features in the grid, but has poor polar appearance and a few faint artifacts (see Supplementary Figure 1). Alternative choices of exponent, or different tension values in the splining method, yield substantially similar results.

149 The rms difference between the chosen (splined T=0.5) dataset and the original data is about 30m : this
150 compares with the estimated accuracy of the original data of typically 100m or so (Stiles et al., 2009;
151 Zebker et al., 2009b). No attempt has been made to apply error-determined weights to the gridding
152 procedure.

153

154 < Figure 3 >

155 The map data are provided as an array of numbers in Supplementary Data file #1. Profiles through the
156 interpolated map are shown in figures 4 and 5 : this shows how the interpolation scheme introduces
157 steep slopes where they are required to agree with the data, and otherwise smoothly joins the points..
158 Figure 6 shows a hypsogram of the interpolated map, and of the original data - it is seen that they are
159 similar, although (as one might expect) the interpolated distribution is slightly narrower since by
160 definition it includes points that are intermediate to the original data.

161 < Figure 4 >

162 < Figure 5 >

163 < Figure 6 >

164 Figure 7 shows a topographic map of the Earth at 1x1^{o} resolution, using the GTOPO5 dataset, and the
165 corresponding map obtained by sampling that data with the same geographical distribution of points as
166 we have available for Titan, and then applying our spline interpolation procedure. This then gives a
167 qualitative impression of how well the data at hand captures the global topographic characteristics of a
168 planet (a related exercise by Lorenz (1996) showed that recognition of a partly-observed landscape
169 improves sharply up to ~30% coverage, with the incremental value of additional coverage only

decreasing above that point). It is seen that while some extremes are not captured the overall shape of the continental land masses (including Greenland and Australia) is identified, together with major mountainous regions (with the exception of the Tibetan plateau). Supplemental figure 2 shows the results of the same exercise for Mars.

Figure 8 indicates the distance in the map to the nearest measurement (provided as a cylindrical map to facilitate lookup of specific coordinates). This map (provided as supplemental data file #2) can serve as a guide for interpretive analyses – clearly one should exercise caution when drawing conclusions about topography for areas distant from where there is actual data. The largest distance is about 1000km (equivalent to ~20^o of latitude along a meridian, or 20^o of longitude at the equator) ; some of these largest gaps may be partly filled by planned future data acquisitions.

4. Maps and Geological Discussion

The map from figure 3 is shown with contours added to facilitate the indication of slope directions in figure 9, together with a VIMS basemap and the original data tracks for reference. The polar regions are shown in stereographic projection in figure 10.

< Figure 9 >

< Figure 10 >

189 The maps, and the data file in Supplemental Information, are given as surface heights relative to a
190 2575km sphere, and thus are suitable for purely geometric work (e.g. occultation timing). For problems
191 relating to gravity, such as hydrology, the ellipsoidal geoid of Iess et al. (2011) should be subtracted to
192 get heights relative to an equipotential. Since the geoid amplitude is only ~100m equator-to-pole, the
193 effects in many cases will not be significant, however.

194 Note that no attempt has been made to force the present topography dataset to be flat in Titan's seas.
195 This is in part to expose the original data (which might afford some insight into how deep the basins
196 might be expected to be), and because the complete extent of Kraken Mare has not yet been
197 determined in radar data, so any attempt to flatten the seas would be somewhat subjective.

198 The fact that Titan's topographic range is only about 2.5km has been noted previously (Lorenz et al.,
199 2011). That paper also noted that the hypsogram appeared negatively skewed, with some exceptional
200 troughs. The map highlights at least one of these (see section 4.2).

201

202 4.1 Overall Pattern

203 The most striking impression overall is that of two equatorial highland provinces, somewhat near the
204 sub- and anti-saturnian points (0° and 180°W, respectively). These were apparent as a prolateness of
205 Titan's figure (Zebker et al., 2009b), in other words a C22 topography term. This topographic bulge is
206 rather in excess of Titan's measured geoid (Iess et al. 2010) and indeed larger than the ~100m tidal
207 bulge that would be expected from hydrostatic equilibrium. The relationship of the long-wavelength
208 topographic variation on Titan to the gravity field is discussed in Nimmo and Bills (2010) who infer a
209 non-convecting ice crust with a thickness that varies with latitude.

Two complex highland regions can be seen spanning the equatorial region. These highland terrains are irregular, with significant entrant depressions and outlying hills. A striking aspect, and one that is a reversal of the common association of optically bright with radar-bright and locally elevated terrain, is that at the large scale, there is a poor correlation of albedo and elevation. While some sand seas like Belet and Fensal are in depressions, others (Shangri-La) are not. Conversely, the southern portion of the well-known bright region Xanadu (Radebaugh et al. 2011) is partly a depression, but is not filled with sand.

The variation in topography across Xanadu from north to south (Figs. 5 and 9) is intriguing (and inconsistent with the interpretation of the western part of Xanadu as having an impact origin (Brown et al., 2011) unless there has been a significant and asymmetric post-formation change in topography). It is, perhaps, interesting that Hotei and Tui Regios which have been suggested to have cryovolcanic origins (e.g. Lopes et al., 2013) both lie within the lower elevation portion of Xanadu. An alternative proposal , consistent with this lower elevation, has been that Tui and especially Hotei are former lake beds, as evidenced by drainage patterns (e.g. Moore and Howard, 2010) and a spectral signature seen elsewhere in lake margins and interpreted to indicate evaporite deposits (Barnes et al., 2011). The contiguous nature of the dune fields from Fensal/Aztlan through Senkyo and Belet and around Adiri to Shangri-La clearly demonstrates that, as expected, while dunes are interrupted (deflected or truncated) by short-wavelength changes in topography (even if the change in elevation is low) they are not affected by even large changes in elevation over long distances, i.e. low slopes.

As the profiles show (figures 4 and 5), steep slopes, and sudden changes in slope, are often encountered. We defer, however, analyses of slope statistics and spectral analysis of topography to future work.

232

233 4.2 Basins for southern seas ?

234 Stofan et al. (2012) have proposed in SAR image data some morphological evidence for wide basins that
235 may be the vestige of prior seas. The concentration of lakes and seas in the north polar region is a
236 remarkable contrast with the south, but seems likely to be an ephemeral situation : the timescale for
237 Croll-Milankovich climate cycles on Titan is ~50,000 years (Aharonson et al., 2009) and thus when
238 humans were migrating out of Africa for the first time, Titan's arctic may have been somewhat dry and
239 large seas may have been present in the south.

240 The topographic data presently in hand points to the lowest point being at 59^{o} S, 317^{o} W. It can be seen
241 (figure 10) by comparing the topography nearby that if a sea were present here in a previous epoch with
242 a spatial extent (~400km) comparable with present-day Ligeia Mare, this sea would have a central depth
243 approaching 1000m.

244 It is notable that the wettest known place in the south (Ontario Lacus, 79^{o}S, 180^{o}W) is not the lowest
245 place - evidently the entire southern polar region is not efficiently connected hydraulically (cf Hayes et
246 al., 2008) and the present liquid in Ontario must have been somewhat locally precipitated. Transient
247 liquids were observed at Arrakis Planitia, 80°S and 120° W (Turtle et al., 2009; Hayes et al., 2011). Both
248 Ontario and Arrakis are in local topographic lows.

249

250 4.3 Fluvial Networks

251 The river channels of Elivagar Flumina drain to the northeast (Lorenz et al., 2008) from near the
252 Menrva impact structure at 20°N, 77°W. (Menrva itself has relatively subdued topography, typical of a

crater of its size (Neish et al., 2013), and hence is not observed in the global topographic map.) The topography map here has something of a discontinuity in that the terrain slopes downwards both north and south of the SARtopo tracks from the T3 flyby that first imaged Menrva and Elivagar. The northeast drainage of Elivagar is consistent with the local topography, which suggests a drop of ~200m in elevation over ~200km in that direction.

Other river channels have been identified (e.g. Burr et al. 2009 ; Lorenz et al. 2008) in Xanadu at around 10S and 125-145°W., draining south. Although the very rugged terrain of Xanadu (Radebaugh et al. 2011) means topography measurements (which could trigger on local mountains) must be interpreted with care, if we take the sensed topography as corresponding to valley-floor elevations, it is reassuring that the topography map indeed shows a southward slope in this area, with in fact a slope of around double that indicated for Elivagar above. This slope difference may be connected with the more incised and developed network in Xanadu compared with the apparently shallow and anabranching/braided arrangement in Elivagar.

4.4 Plateaus

Isolated mountains and mountain belts on Titan seen in SAR imaging have been discussed previously (e.g. Mitri et al., 2010). A striking discovery in the southeastern quadrant of the topography map (see figure 11) is an arc of four prominent topographic rises, labeled A, B, C, D. Each is about 200km wide and stands ~700m higher than the surrounding terrain. Inspection of the SAR images with the raw topography data overlain for A, B and D shows that the highland terrain is radar-bright and heavily dissected by fluvial valleys. C is only observed in altimetry at present. A, B, and C occur on or near areas

that are seen to be darker at 940-nm (Fig. 4). The coordinates and elevations above the 2575km datum are A: 49°S, 150°W, 380m; B 35°S, 100°W, 240m; C 36°S, 63°W, 260m; D 48°S, 12°W, 350m. The arrangement of these features draws the eye, but it is unclear if there is any global tectonic relationship between them. Note that some arc-shaped features are apparent in the upper left quadrant of the map product : these are a result of real data - they correspond to short-wavelength variations between the topography in swaths TA and T3 - so 'artifacts' is perhaps not quite an accurate term. However, the arc-shaped arrangement of the plateaus A,B,C,D was not produced in the same way - each feature was observed in a different datatake.

5. Conclusions

A topographic map has been assembled and interpolated from available Cassini radar data using splining with appropriate regridding around the poles. This map is made available to the community as a gridded dataset for correlative and other studies. Notable features are the overall anticorrelation between elevated terrain and optically dark terrain (contrary to what has been observed at smaller scales), prominent depressions in the south polar regions that may be relict seabeds, the slopes driving large-scale river systems, and the presence of four isolated highland features in southern mid-latitudes.

Acknowledgements

294 This work was supported by the Cassini/Huygens mission, which is a joint endeavor of NASA, the
295 European Space Agency (ESA), and the Italian Space Agency (ASI) and is managed by JPL/Caltech under a
296 contract with NASA.

297

298 References

299

300 Aharonson O., M. T. Zuber, and D. H. Rothman, Statistics of Mars' Topography from the Mars Orbiter
301 Laser Altimeter: Slopes, Correlations, and Physical Models, J. Geophys. Res., 106, 23,723-23,735, 2001.

302 Aharonson, O., Hayes, A., Lunine, J. I., Lorenz, R. D., Elachi, C., 2009. An asymmetric distribution of lakes
303 on Titan as a possible consequence of orbital forcing, Nature Geoscience, 2, 851-854

304 Barnes, J.W., Bow, J., Schwartz, J. Brown, R.H., Soderblom, J.M., Hayes, A.G., Vixie, G., Le Moulec, S.,
305 Rodriguez, S., Sotin, C., Jaumann, R., Stepha, K, Soderblom, L. A., Clark, R. N., Buratti, B.J., Baines, K.H.,
306 Nicholson, P.D.,2011. Organic sedimentary deposits in Titan's dry lakebeds: Probable evaporites, Icarus,
307 216, 136-140.Brown, R.H., Barnes, J.W., Melosh, H.J. 2011. On Titan’s Xanadu region. Icarus, 214, 556-
308 560.

309 Burr, D. M., R. E. Jacobsen, D. L. Roth, C. B. Phillips, K. L. Mitchell and D. Viola, 2009. Fluvial network
310 analysis on Titan: Evidence for subsurface structures and west-to-east wind flow, southwestern Xanadu,
311 Geophysical Research Letters, 36, L22203, doi:10.1029/2009GL040909

312 Hayes, A., O. Aharonson, K. Lewis, K. Mitchell, R. Lorenz, P. Callahan,J. Lunine, R. Lopes, S. Wall, C. Elachi,
313 G. Mitri, R. Kirk, Y. Gim, E. Stofan, and the Cassini RADAR Team, 2008. Hydrocarbon Lakes on Titan:
314 Distribution and Interaction with a Porous Regolith, Geophysical Research Letters, 35, L09204,
315 doi:10.1029/2008GL033409

316 Hayes, A. G., O. Aharonson, J. Lunine, R. Kirk, H. Zebker, L. Wye, R. Lorenz, E. Turtle, P. Pail lou, G. Mitri,
317 S. Wall, E R. Stofan, C. Elachi, and The Cassini RADAR Team, 2011. Transient Surface Liquid on Titan from
318 Cassini. Icarus, 211, 655-671

Kirk, R. L., E. Howington-Kraus, B. L. Redding, T. L. Becker, E. M. Lee, B. W. Stiles, S. Hensley, A. G. Hayes, R. M. Lopes, R. D. Lorenz, Karl L.Mitchell, J. Radebaugh, F. Paganelli, L. A. Soderblom, E. R. Stofan; S. D. Wall, High Resolution Topographic Models of Titan's Surface Derived by Radar Stereogrammetry with a Rigorous Sensor Model, Icarus, submitted

Lopes, R.M.C., R. L. Kirk, K.L. Mitchell, A. LeGall, J. W. Barnes, A. Hayes, J. Kargel, L. Wye, J. Radebaugh, E.R. Stofan, M. Janssen, C. Neish, S. Wall, C.A. Wood, J.I. Lunine, M. Malaska. Cryovolcanism on Titan: New results from Cassini RADAR and VIMS, 2013. J. Geophys. Res. Planets, 118, 1-20, doi:10.1002/jgre.20062

Lorenz, R. D. 1996. Characterization of a Planet: Dependence on Coverage Fraction, 27th Lunar and Planetary Science Conference, Houston, TX, March 1996, 773-774

Lorenz, R. D. and J. Radebaugh, 2009. Global Pattern of Titan's Dunes : Radar Survey from the Cassini Prime Mission, Geophysical Research Letters, 36, L03202, doi:10.1029/2008GL036850

Lorenz, R D., R. M. Lopes, F. Paganelli, J.I. Lunine, R. L. Kirk, L.. A. Soderblom, E. Stofan, G. Ori, M. Myers, H. Miyamoto, B. Stiles, S. D. Wall, C. A. Wood, and the Cassini RADAR Team, 2008, Fluvial channels on Titan: Initial Cassini RADAR observations,, Planetary and Space Science, 56, 1132-1144

Lorenz , R. D., E. P. Turtle, B. Stiles, A. Le Gall, A. Hayes, O. Aharonson, C. A. Wood, E. Stofan, R. Kirk, 2011. Hypsometry of Titan, Icarus, 211, 699-706

Mitri, G., M. T. Bland, A. P. Showman, J. Radebaugh, B. Stiles, R. M. C. Lopes, J. I. Lunine, R. T. Pappalardo, 2010. Mountains on Titan: Modeling and observations, Journal of Geophysical Research, 115, CiteID E10002, doi: 10.1029/2010JE003592

339 Moore, J.M. and A.D. Howard (2010), Are the basins of Titan's Tui Regio and Hotei Regio sites of former
340 low latitude seas? Geophys. Res. Lett., 37, L22205, doi:10.1029/2010GL045234.

341 Neish, C. D., R.L. Kirk, R.D. Lorenz, V.J. Bray, P. Schenk, B. Stiles, E. Turtle, K. Mitchell, A. Hayes, and the
342 Cassini RADAR Team, 2013. Crater topography on Titan: Implications for landscape evolution. Icarus,
343 223, 82-90

344 Nimmo, F. and B. G. Bills 2010. Shell thickness variations and the long-wavelength topography of Titan,
345 Icarus, 208, 896-904

346 Radebaugh, J., Lorenz, R. D., Wall, S. D., Kirk, R. L., Wood, C. A., Lunine, J. I., Stofan, E. R., Lopes, R. M. C.,
347 Valora, P., Farr, T. G., Hayes, A., Stiles, B., Mitri, G., Zebker, H., Janssen, M., Wye, L., Legall, A., Mitchell,
348 K. L., Paganelli, F., West, R. D., Schaller, E. L. and the Cassini RADAR Team, 2011. Regional
349 geomorphology and history of Titan's Xanadu province, Icarus, 211, 672-685

350 Smith, D. E. and M. T. Zuber, 1996. The Shape of Mars and the Topographic Signature of the
351 Hemispheric Dichotomy, Science, 271, 184-188

352 Smith, W. H. F. and P. Wessel, 1990. Gridding with continuous curvature splines in tension, Geophyics,
353 55, 293-305

354 Stiles, B. W., S. Hensley, Y. Gim, D. M. Bates, R. L. Kirk, A. Hayes, J. Radebaugh, R. D.Lorenz, K. L.
355 Mitchell, P. S. Callahan, H. Zebker, W. T. K. Johnson, S. D. Wall, J. I. Lunine, C. A. Wood, M. Janssen, F.
356 Pelletier, R. D. West, C. Veeramacheneni, and the Cassini RADAR Team, 2009. Determining Titan Surface
357 Topography from Cassini SAR Data, Icarus, 202, 584-598

358 Stofan, E. R., Aharonson, O., Hayes, A. G., Kirk, R., Lopes, R., Lorenz, R. D., Lucas, A., Lunine, J. I.,
359 Malaska, M., Radebaugh, J., Stiles, B. W., Turtle, E. P., Wall, S. D., Wood, C. A., Cassini Radar Team 2012.

Searching for the Remnants of Southern Seas: Cassini Observations of the South Pole of Titan, American Astronomical Society, DPS meeting #44, #201.08

Tokano, T., 2010. Relevance of fast westerlies at equinox for the eastward elongation of Titan's dunes, Aeolian Research, 2, 113-127.

Turtle E.P., Perry J.E., McEwen A.S., DelGenio A.D., Barbara J., West R.A., Dawson D.D., Porco C.C., 2009. Cassini Imaging of Titan's High-Latitude Lakes, Clouds, and South-Polar Surface Changes, GRL 36, L02204, doi:10.1029/2008GL036186.

Wall, S. D., Lopes, R. M., Stofan, E. R., Wood, C. A., Radebaugh, J. L., Stiles, B. W. , Nelson, R. M., Kamp, L. W., Janssen, M. A., Lorenz, R. L., Lunine, J. I., Farr, T. G., Mitri, G., Paillou, P., and Mitchell, K. L., 2009. Cassini RADAR images at Hotei Arcus and western Xanadu, Titan: evidence for geologically recent cryovolcanic activity, Geophysical Research Letters, 36, L04203, doi:10.1029/2008GL036415

Zebker, H.A., Stiles, B., Hensley, S., Lorenz, R., Kirk, R.L., Lunine, J., 2009a. Size and shape of Saturn's moon Titan from Cassini Radar altimeter and SAR monopulse observations. Science 324, 921–923.

Zebker, H.A., Gim, Y., Callahan, P., Hensley, S., Lorenz, R., and the Cassini Radar Team, 2009b. Analysis and interpretation of Cassini Titan Radar Altimeter echoes. Icarus 200, 240–255

Figure Captions

Figure 1. Topography data coverage on a sinusoidally projected 940nm albedo map of Titan, centered on the 180° meridian. (a) Altimetry swaths – note the T77 swath along the equator just right of center, and the long T30 swath at the upper right edge. (b) The much more extensive SARtopo coverage.

Figure 2. Surface heights in 1x1° bins from SARtopo (small circles) and altimetry (triangles). Both datasets show the oblateness of Titan. (Cf. profiles along lines of latitude in Fig. 5 and longitude in Fig. 6.)

Figure 3. Interpolated topography. These data are in Supplementary Data file #1, and are plotted with contours in figure 9. The influence of the original data can be seen in some changes of slope, and that large areas are present where no short-wavelength topography is seen (because there are no data to indicate it).

Figure 4. Surface height profiles along lines of latitude. The length of the plots is scaled such that the physical length scale is the same (the latitude circle at 60^{o} North or South is half of the 16,180km length at the equator). The solid line is the interpolated topography field, circles denote SARtopo measurements and triangles show altimetry measurements. Titan's prolate shape is evident as a wavenumber-2 variation with longitude, most prominent at 30^{o}N and at the equator, with local maxima near the prime meridian.

Figure 5. As for figure 4, but profiles along meridians from the south pole at left to north pole at right. Titan's polar depressions are particularly evident at the prime meridian.

Figure 6. Hypsogram of the source data, and of the splined map. The splined map is narrower, by definition, since it contains many interpolated values.

Figure 7. A cylindrical map of Earth topography. Top panel is the full dataset (at 0.5x0.5^{o} resolution) whereas the lower panel is the estimated topography field obtained by downsampling to 1x1^{o}, extracting data from that grid at those coordinates where we have Titan data, and performing the spline interpolation as described in the text. The major ocean basins and continental land masses (including Greenland and Australia) are identified, together with major mountainous regions (with the exception of the Tibetan plateau, which did not happen to lie on a datatake.)

Figure 8. Distance to the nearest measured height. The cylindrical projection is the same as for other maps. These data are in supplemental data file #2.

Figure 9. Cylindrical Maps. Upper panel is a VIMS multispectral basemap with gold-colored radar imaging where coverage exists and color-coded topography where that data are present. The lower panel shows the same interpolated topography field as figure 3, but with 200m contours added to facilitate interpretation. The south polar depressions, and four mountains (see figure 11) are notably prominent. A dark region at 50-65°S, 300-360°W coincides with a major depression. It is striking that there is in fact an anticorrelation with albedo at the largest scales, wherein some sand seas are not in large depressions but are most extensive at the pro- and anti-saturnward bulges.

Figure 10. Polar Topography Maps (bottomleft North, right , South) in stereographic projection, with VIMS/radar maps (top) for comparison. Note the deep basins at 72^{o}S, 340^{o}W and the wider basin at 68^{o}S, 255^{o}W. Ontario Lacus (72^{o}S 183^{o}W) is reassuringly seen to be in a depression, but it is notable that it is by far not the lowest area. Arrakis Planitia (80°S, 120°W) is also found within a local depression. Contour lines are at 200m intervals.

Figure 11. Upper left is a cyclindrical projection of the southeast quadrant of the topography map, highlighting 4 major topographic rises A-D. The insets show SAR images at 1.3km/pixel with the original

420 SARtopo or altimetry datapoints overlain. In each case seen (A,B,D) the highland terrain is radar-bright
421 and heavily dissected by fluvial valleys. C is only observed in altimetry at present.

422

lorenz_topomap_fig01.tif
Click here to download high resolution image

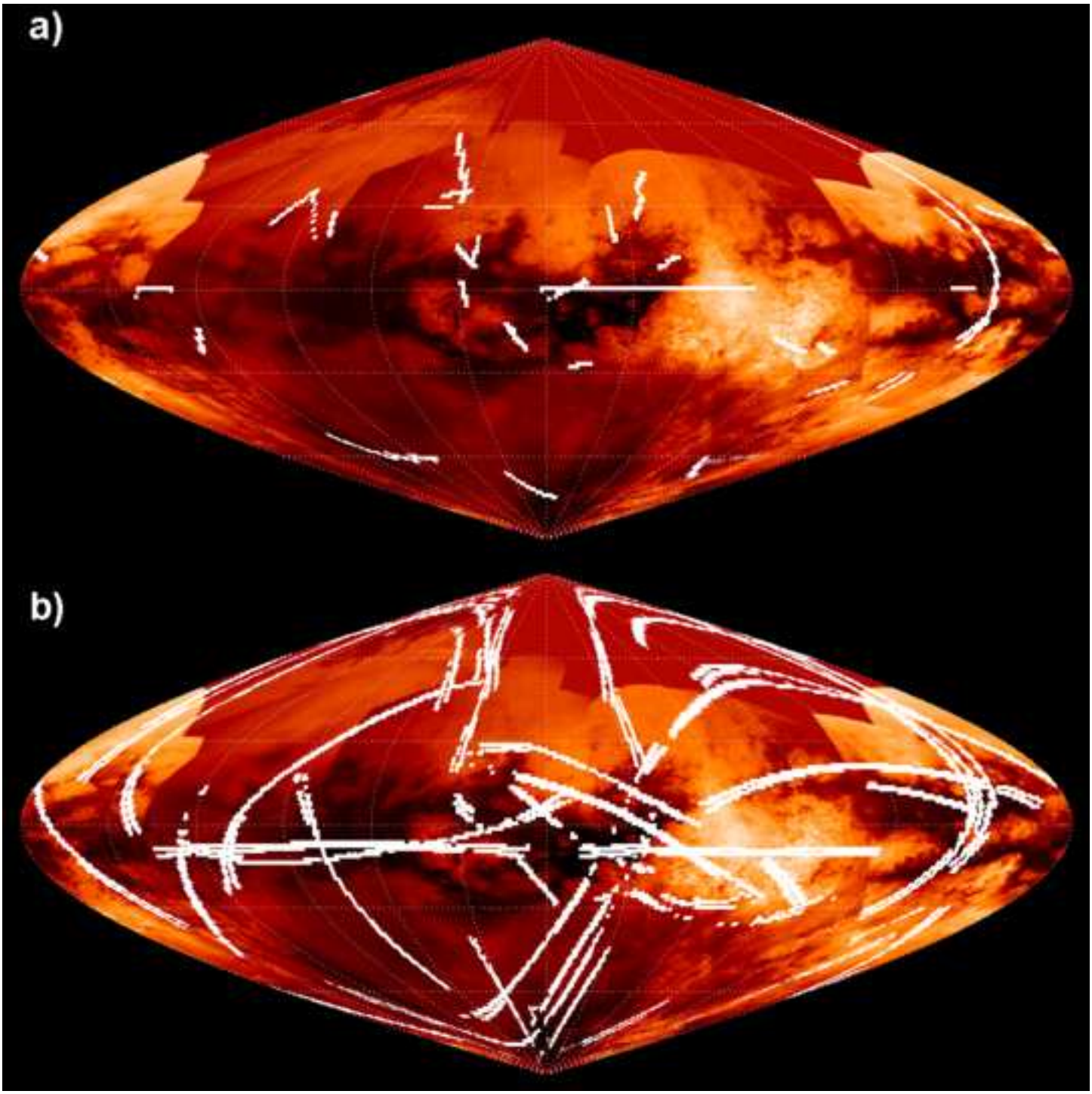

lorenz_topomap_fig02.tif
Click here to download high resolution image

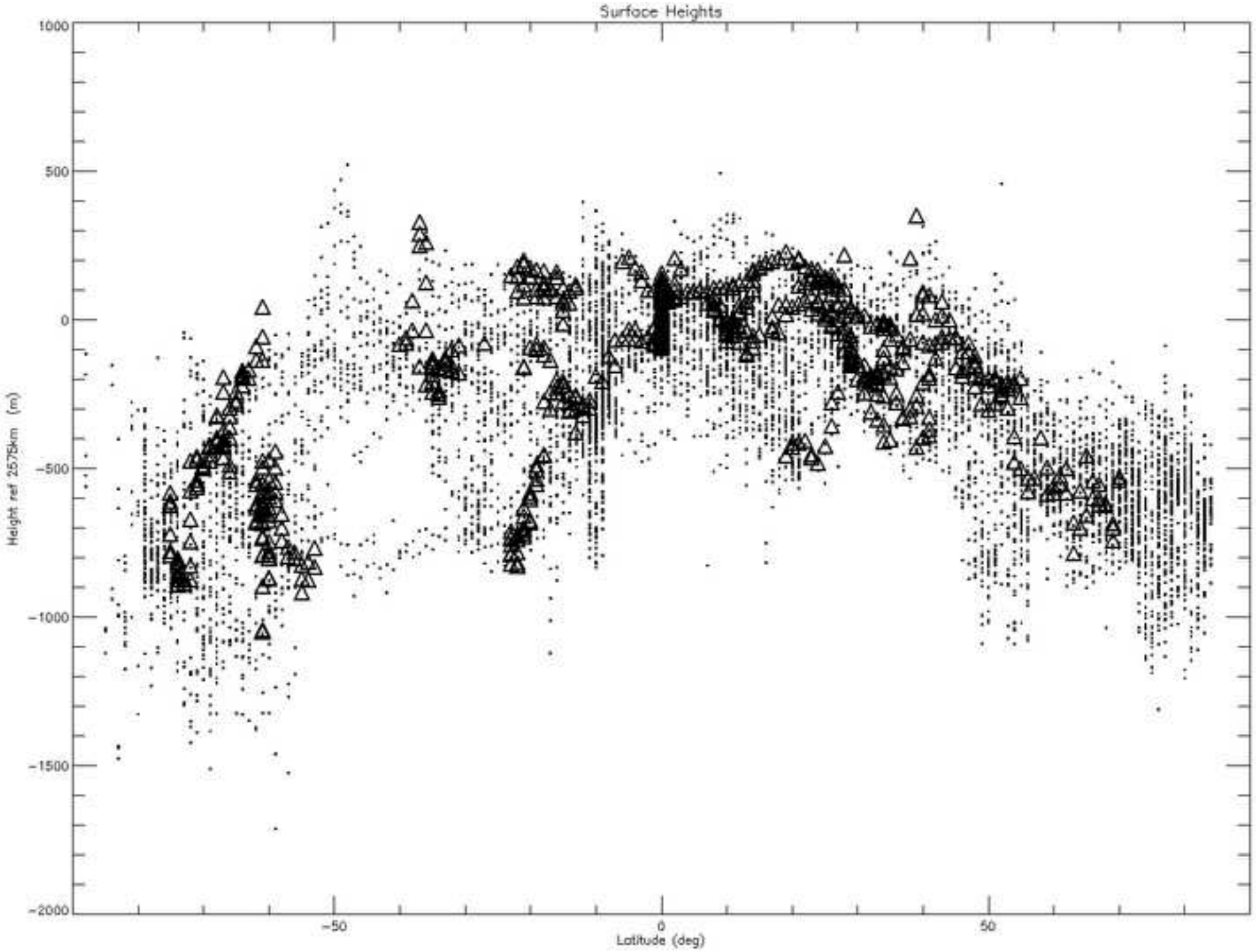

lorenz_topomap_fig03_cyl_nocontour.tif
Click here to download high resolution image

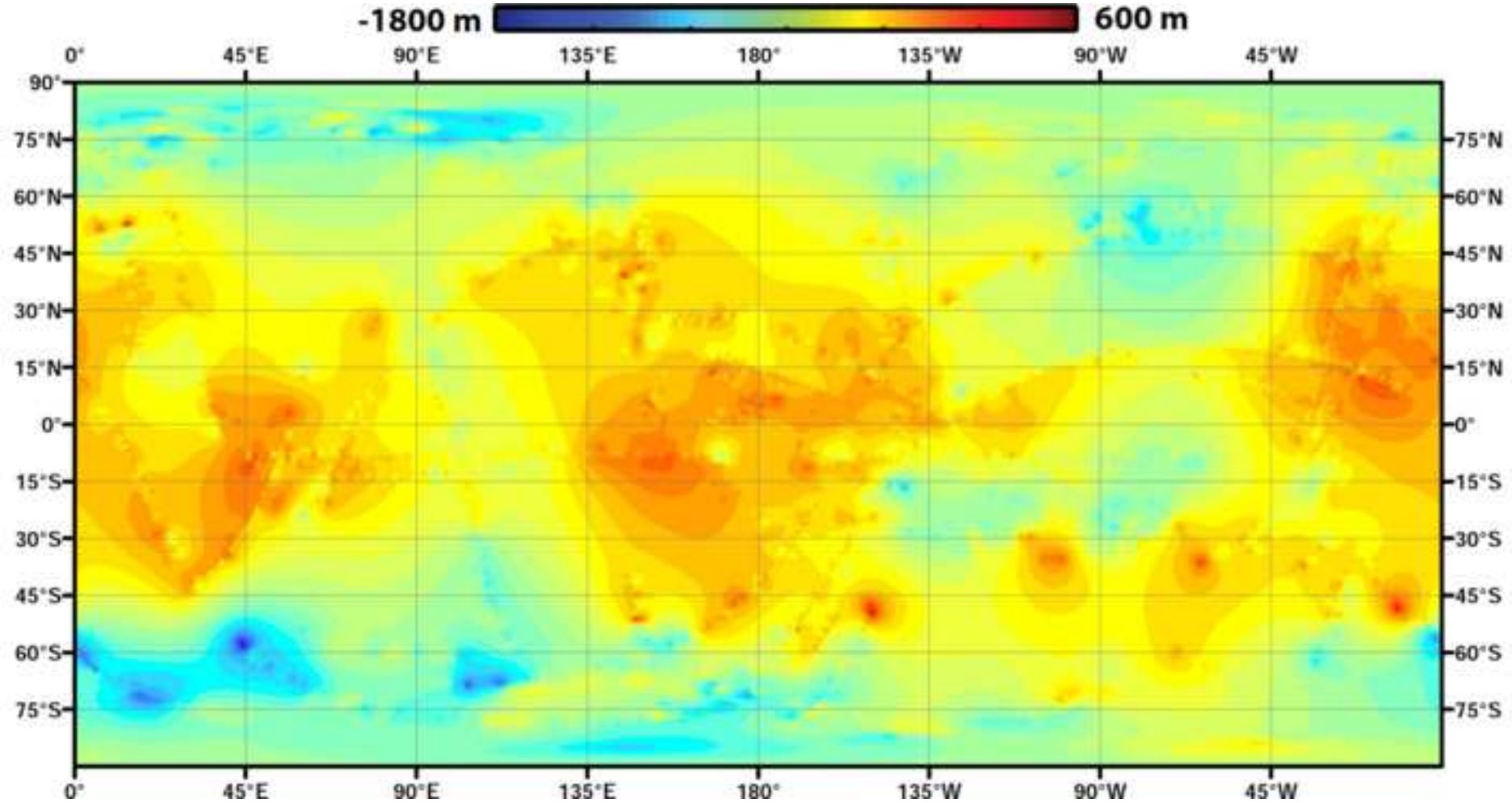

lorenz_topomap_fig04.tif
Click here to download high resolution image

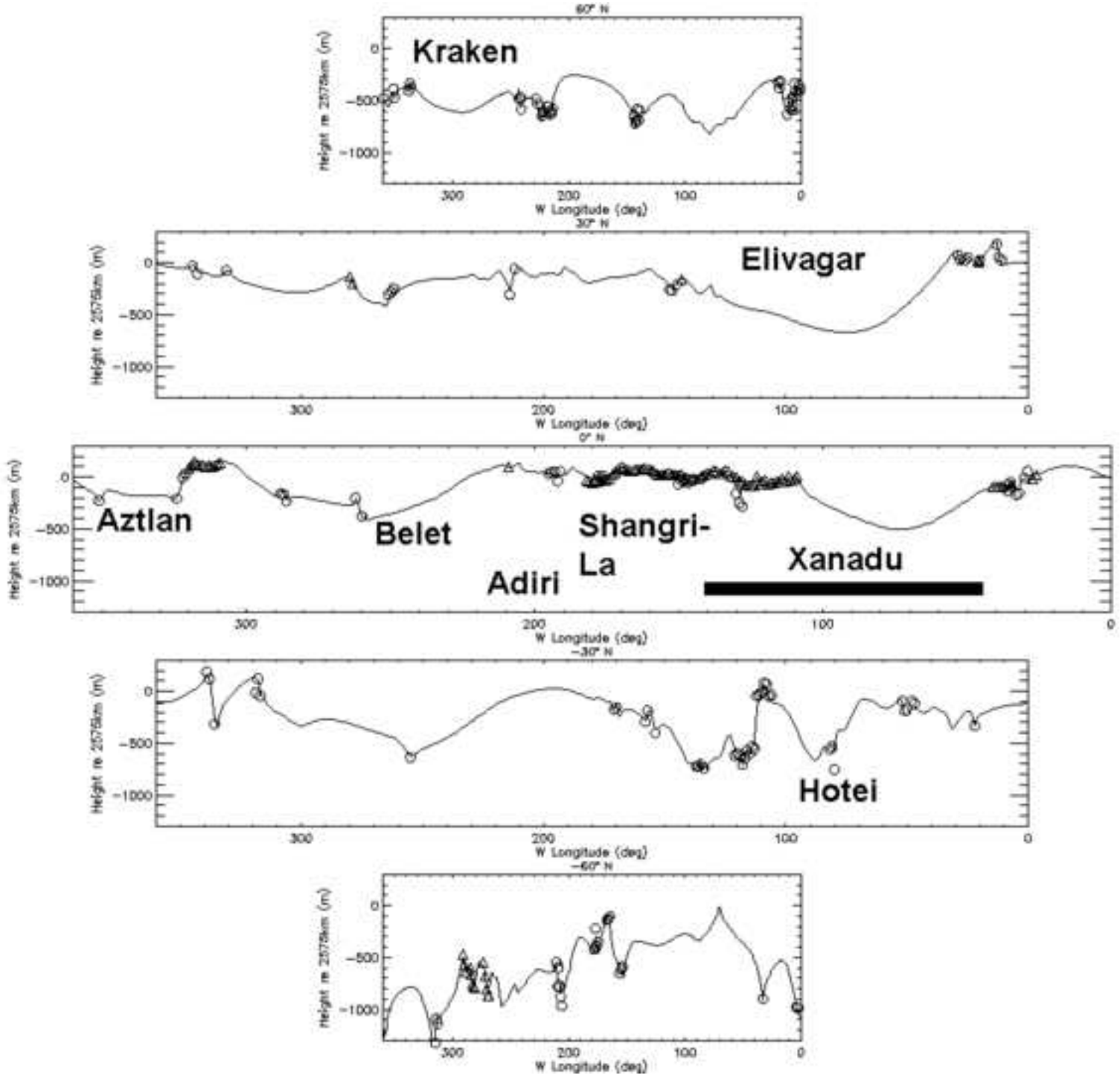

lorenz_topomap_fig05.tif
Click here to download high resolution image

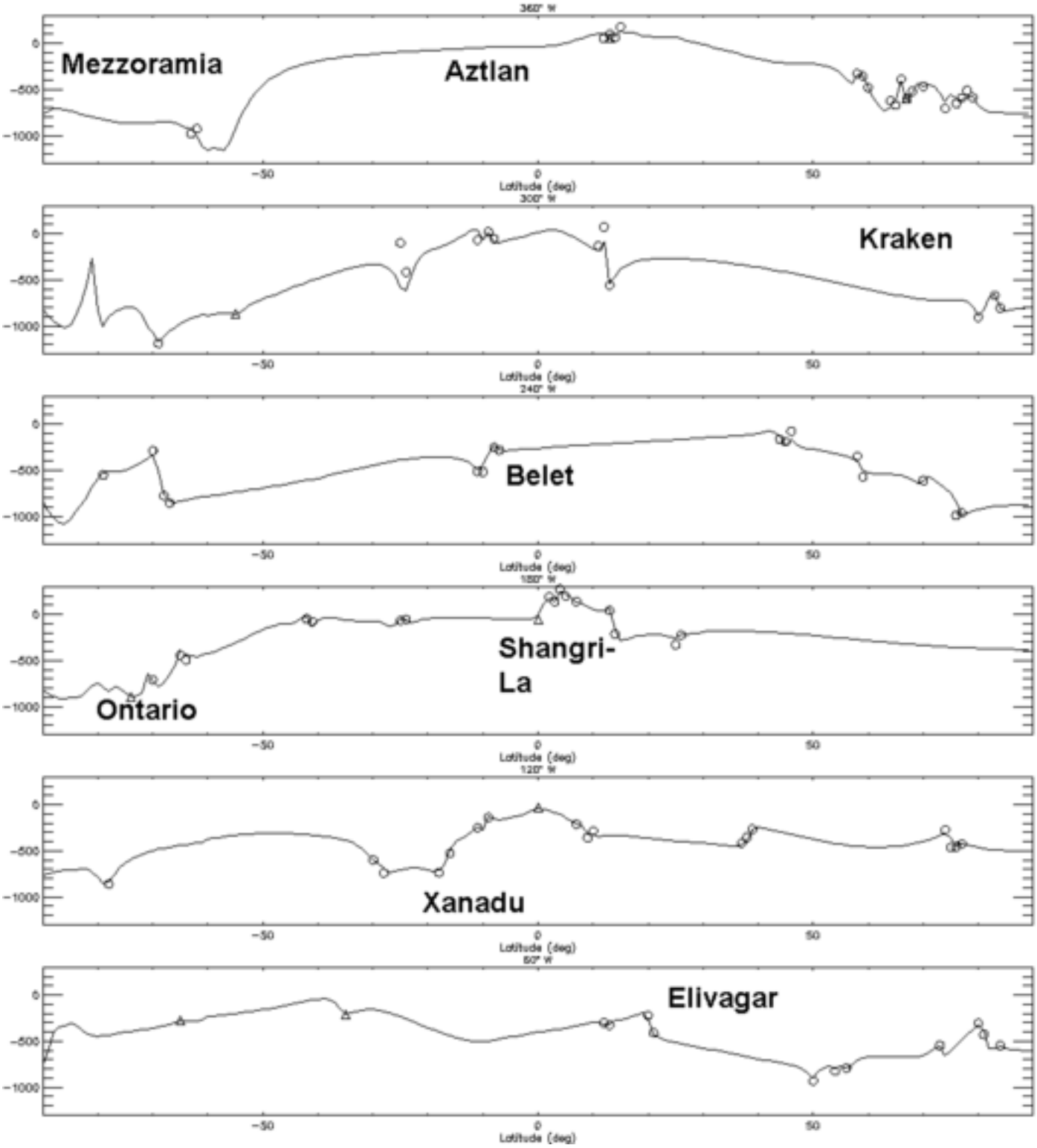

lorenz_topomap_fig06.tif
Click here to download high resolution image

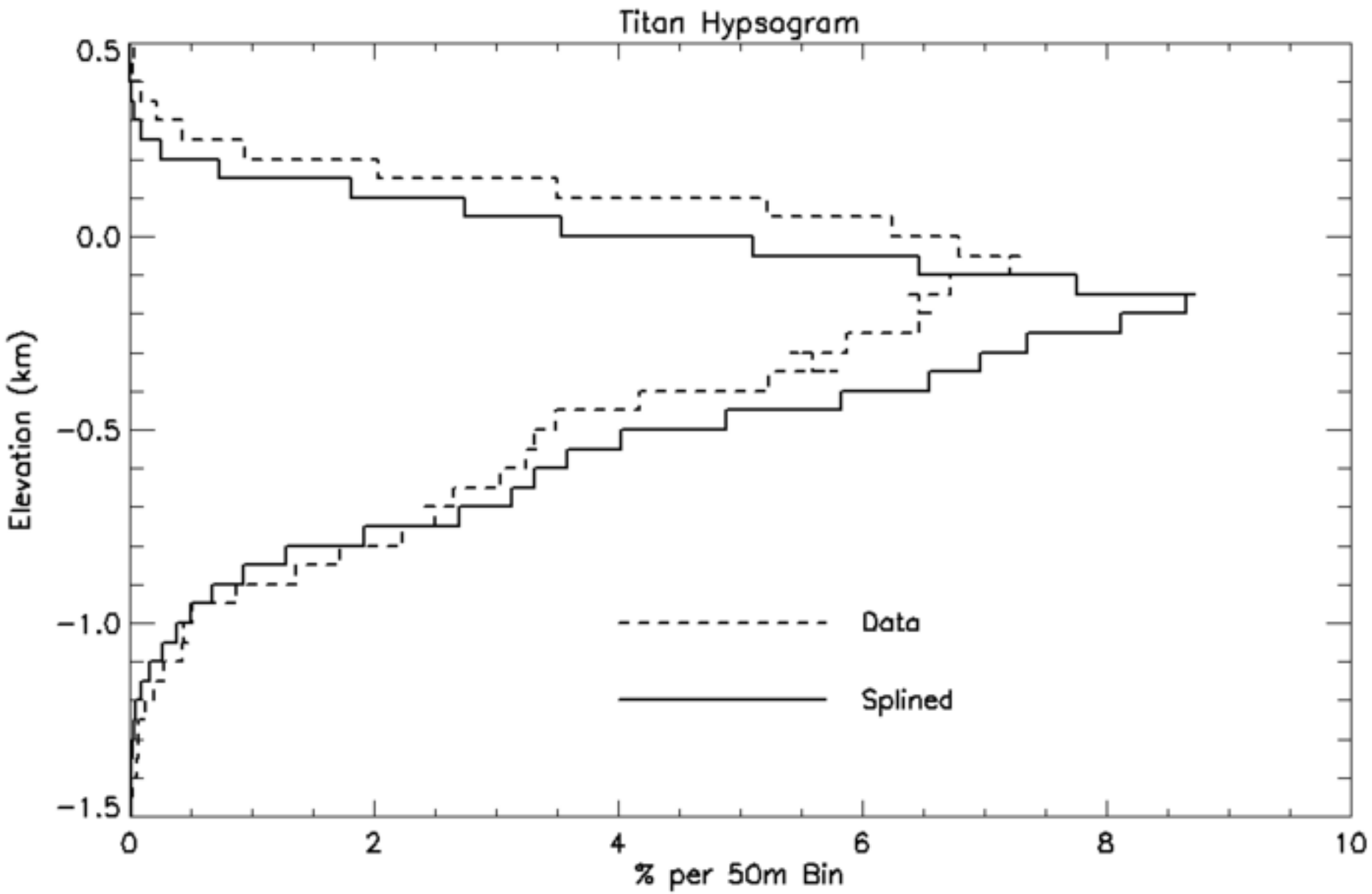

lorenz_topomap_fig07new_earthsampled.tif
Click here to download high resolution image

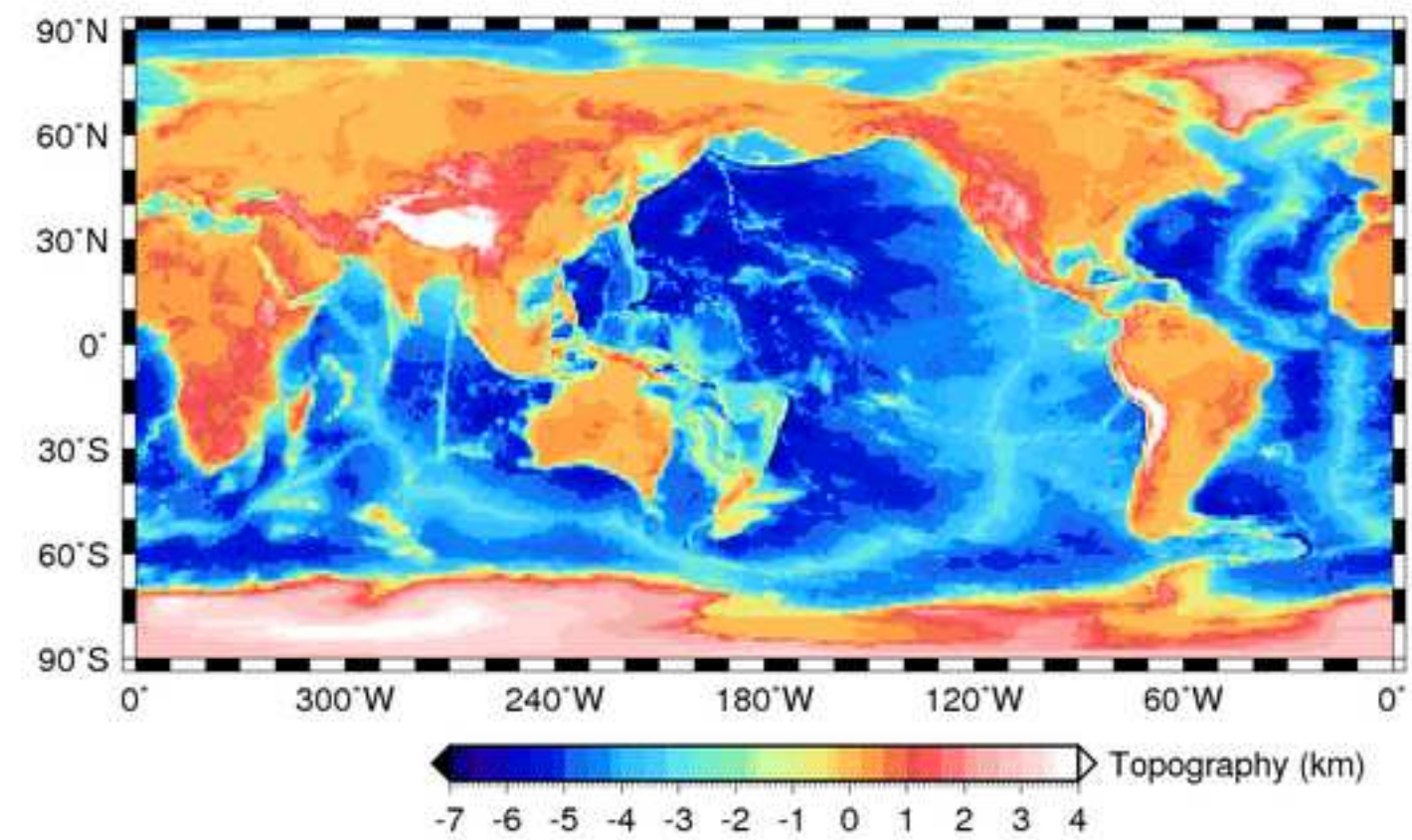

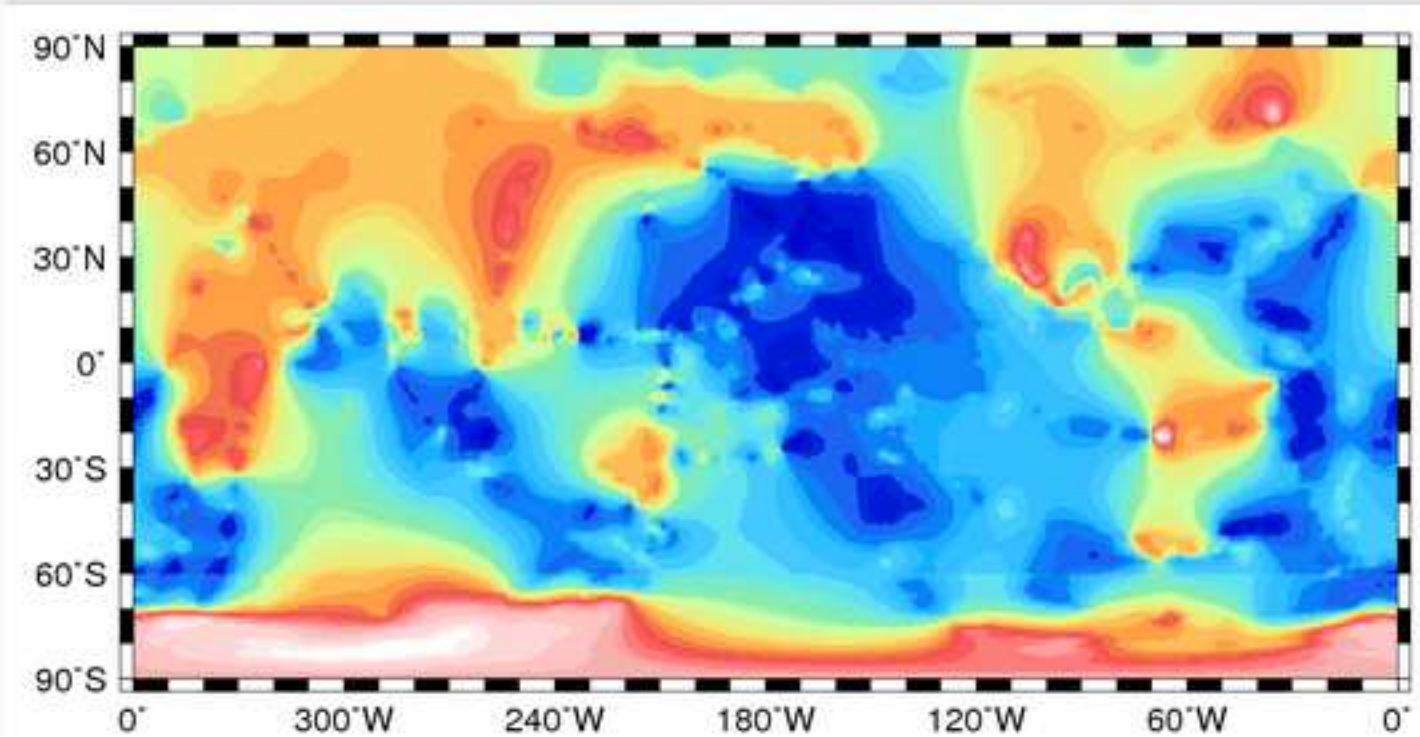

lorenz_topomap_fig08_distancemap.tif
Click here to download high resolution image

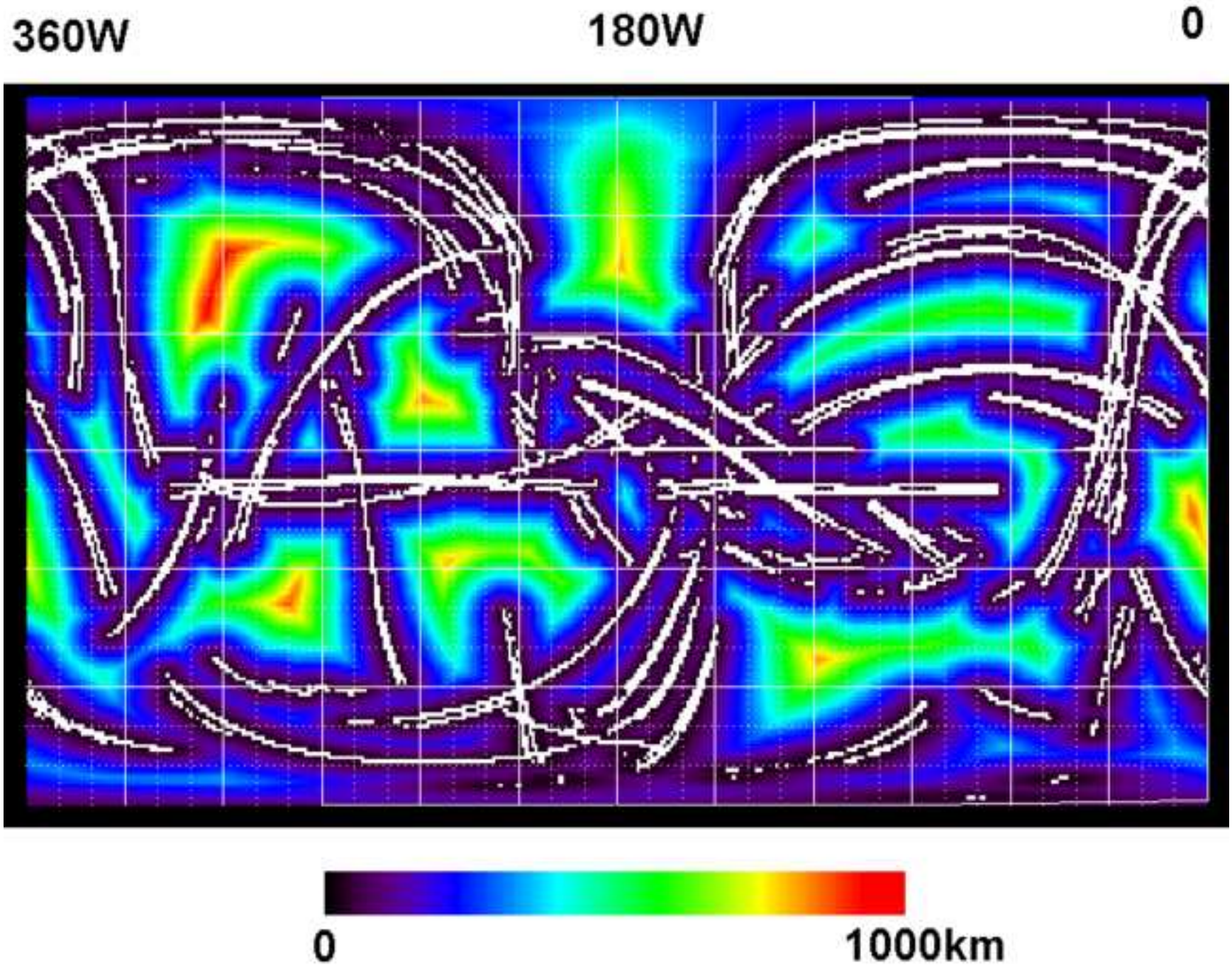

lorenz_topomap_fig09_cyl_contour.tif
Click here to download high resolution image

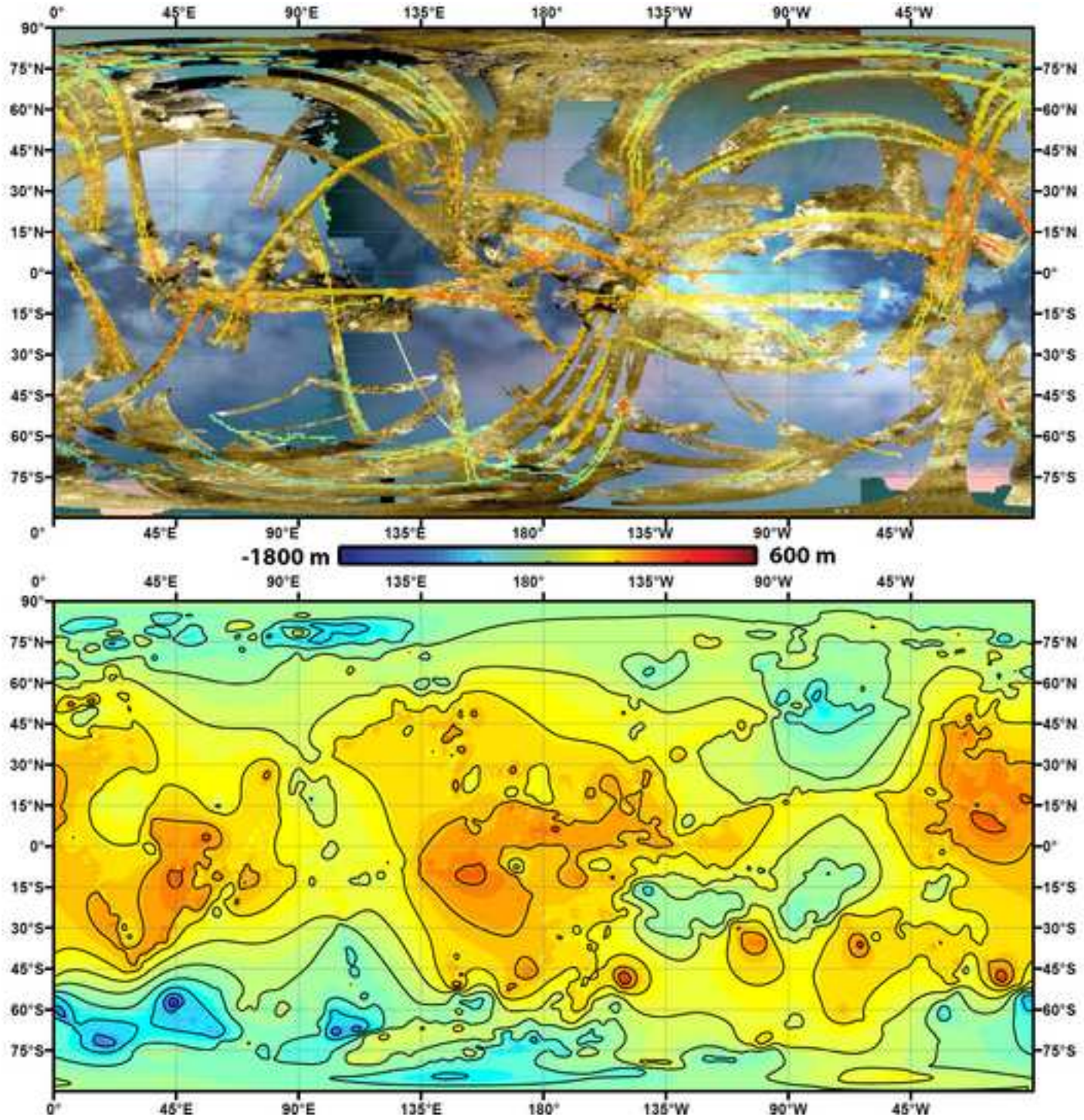

lorenz_topomap_fig10_polar_contour.tif
Click here to download high resolution image

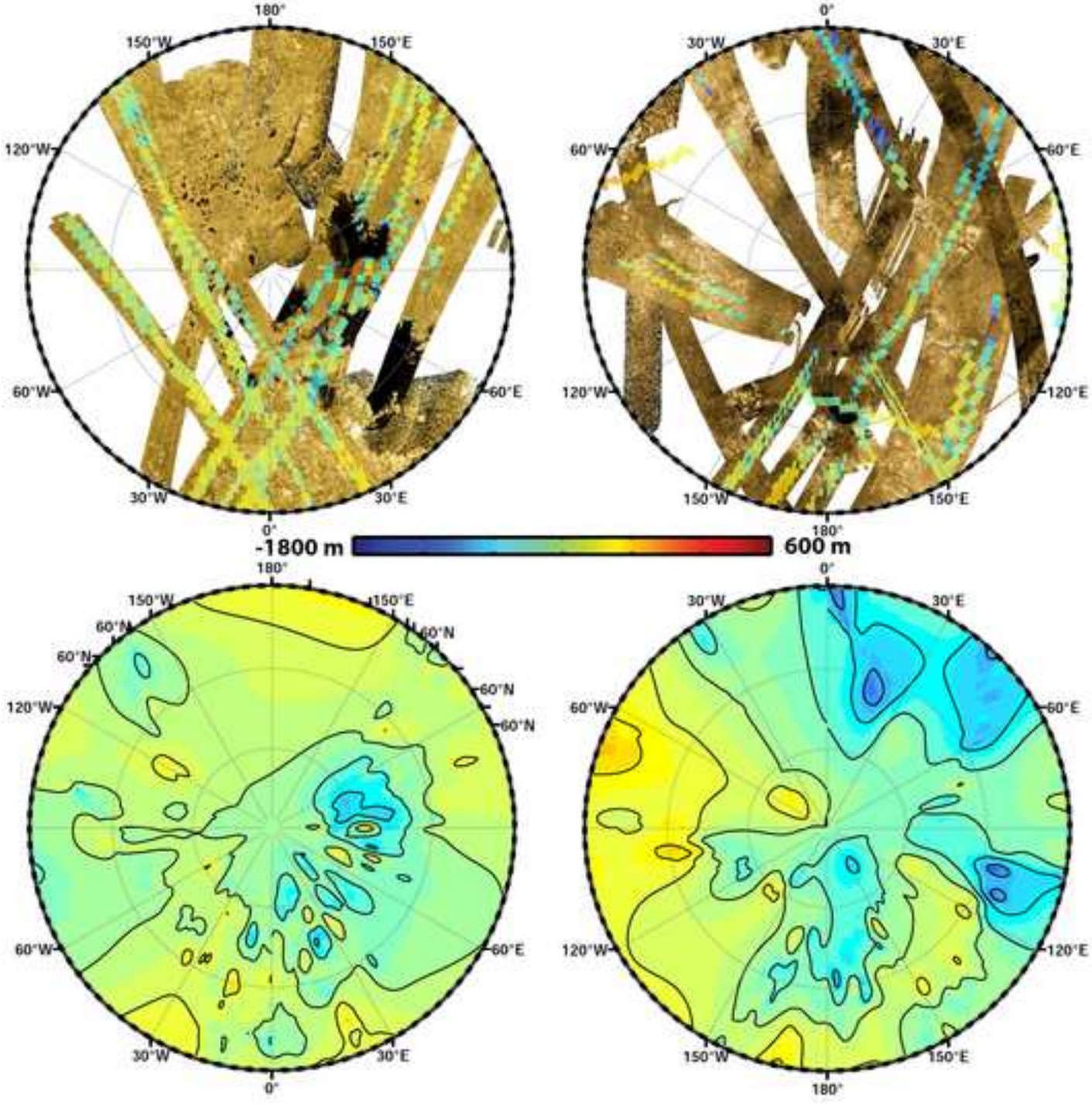

lorenz_topomap_fig11.tif
Click here to download high resolution image